Scientific Research Publishing

Computational Molecular Bioscience, 2020, 10, 111-128
https://www.scirp.org/journal/cmb
ISSN Online: 2165-3453
ISSN Print: 2165-3445

Molecular Docking and Conceptual DFT-Based Study of Some Potential SARS-CoV-2 Inhibitors

Norma Flores-Holguín, Daniel Glossman-Mitnik

Laboratorio Virtual NANOCOSMOS, Departamento de Medio Ambiente y Energía, Centro de Investigación en Materiales Avanzados, Miguel de Cervantes 120, Complejo Industrial Chihuahua, Chihuahua, Mexico
Email: norma.flores@cimav.edu.mx, daniel.glossman@cimav.edu.mx

How to cite this paper: Flores-Holguín, N. and Glossman-Mitnik, D. (2020) Molecular Docking and Conceptual DFT-Based Study of Some Potential SARS-CoV-2 Inhibitors. *Computational Molecular Bioscience*, **10**, 111-128.
https://doi.org/10.4236/cmb.2020.104008

Received: November 12, 2020
Accepted: December 28, 2020
Published: December 31, 2020

Abstract

Nowadays, the main effort of the scientific community is focused on the search of specific drugs for the inhibition of the Severe Acute Respiratory Syndrome—Coronavirus 2 (SARS-CoV-2), which is responsible for the Coronavirus Disease 19 or COVID-19. With the same objective in mind, a Molecular Docking study was performed in this work in order to discover information about some antiviral drugs of common use as protease inhibitors. As a complement of this research, a chemical reactivity study of these potential drugs was done with the aim of finding a relationship between the inhibition ability and the chemical reactivity. The results presented in this research constitute one of the first predictions aimed to identify the best potential compounds for this purpose while at the same time verifying the validity of the employed theoretical and computational methodology. By means of the analysis of the number of hydrogen bonds as well as the binding energies coming from the Molecular Docking study, it can be said that Telaprevir, Nelfinavir and Indinavir have the highest probability of success as potential inhibitors of SARS-CoV-2.

Keywords

SARS-CoV-2, Molecular Docking, DFT, Binding Energy, Conceptual DFT

1. Introduction

During the rapid development of the COVID-19 disease, researchers over the whole world are hard-working in order to develop a successful therapy. The main protease proteins of SARS-CoV-2 have been identified as the drug targets required to process the translation of the proteins from the RNA virus. In particular, the main protease (Mpro, also known as 3CLpro) is one of the coronavi-

rus nonstructural proteins (Nsp5) designated as a potential target for drug development [1] [2] [3]. Thus, inhibition of Mpro would prevent the virus from replication and therefore constitutes one of the potential anticoronaviral strategies [1] [2] [3] [4]. For these reasons, the main objective of some of recent investigations has been finding adequate drugs with inhibitory activity properties of this particular protease protein [3]-[9].

Viral proteases show differences depending on the type of virus that express them. Among other aspects, they may vary in their substrate specificity as well as in their amino acid sequences and their subunits. However, all of them have a series of regions of substrate specificity where they can act as receptors, the so-called active center [10]. In order to find the particular region of one of the main proteases of SARS CoV-2 as well as the interactions with the amino acids present in these areas, a Molecular Docking process with molecules with potential inhibition activity can be developed with the aim of finding information about the protein-substrate interactions. With the objective of identifying if already well-known drugs can be used to treat this new disease that nowadays is affecting more than 200 countries and territories around the world [11], a series of protease inhibitors that could block the activity of the SARS-CoV-2 protease enzyme can be tested by using Molecular Docking strategies. These kinds of systems work by blocking the division of the large polyproteins into the smaller fragments that are necessary for the assembling of new viral particles [1] [2] [3] [4].

In the drug discovery research, the identification and validation of lead compounds and the determination of active binding sites of biological targets related to a certain lead compound performed through wet lab experiments are quite expensive and time consuming [12]. Computational determinations reduce effectively the time required to obtain useful drugs and decrease their associated economic costs, making it possible the proposal of new potential drugs with low expenditures and selective targeting [13].

Considering these facts, the overall goal of this research is the discovery of significant binding affinities between some protease inhibitors and a selected protein chosen as the receptor, considering it in a rigid conformation and docking the protease inhibitors into its active site. Once the enzyme-substrate interaction is selected, the binding site at several discrete points is tested and the interaction energies between the molecules and the atoms within the receptor are calculated. This information is used to identify energetically favourable and unfavourable regions for specific ligand-receptor interactions that could guide a correct pharmacophore feature placement or aid in the ligand design and optimization [14] [15] [16].

The selection of the protease inhibitors to be tested in this research was inspired by the recently experimental evaluation of their antiviral activity by Yamamoto and coworkers [17]. The selected molecular systems are Amprenavir, Asunaprevir, Atazanavir, Darunavir, Fosamprenavir, Indinavir, Lopinavir, Nel-

finavir, Ritonavir, Saquinavir, Telaprevir and Tipranavir have been taken from the ZINC15 database [18] of the Food and Drug Administration (FDA) because they are currently used as protease inhibitors against Human Immunodeficiency Virus (HIV) and Hepatitis C Virus [19]-[27], while the crystallographic structure of the SARS-CoV-2 main protease was obtained from Protein Data Bank (PDB) with code 6M03 [28]. The physical and chemical properties of these molecules as well as their pharmacokinetics are readily available through the free online PubChem database (https://pubchem.ncbi.nlm.nih.gov/). A graphical representation of the two-dimensional structures of the considered molecules is displayed in **Figure 1**.

In a complementary way, the chemical reactivity properties of the potential inhibitors were determined through a calculation of the reactivity descriptors that arise from Conceptual Density Functional Theory (CDFT) [29] [30] [31] [32]. The chemical reactivity descriptors affect the selectivity of the molecular system and play an important role in the prediction of the electrodonating or electroaccepting character of the systems [32]-[39]. The electronic configuration details help to describe the recognition process under negative and positive charges, exposing those interactions that can be difficult to identify with non bonded interactions [40]. The use of the concepts derived from this theory as well as their associated descriptors allowed us to find the reactivity of the molecular systems in terms of their electronic densities which was an additional contribution in the validation of the lead compounds. The determination of the Conceptual DFT-based chemical reactivity descriptors of the potential SARS-CoV-2

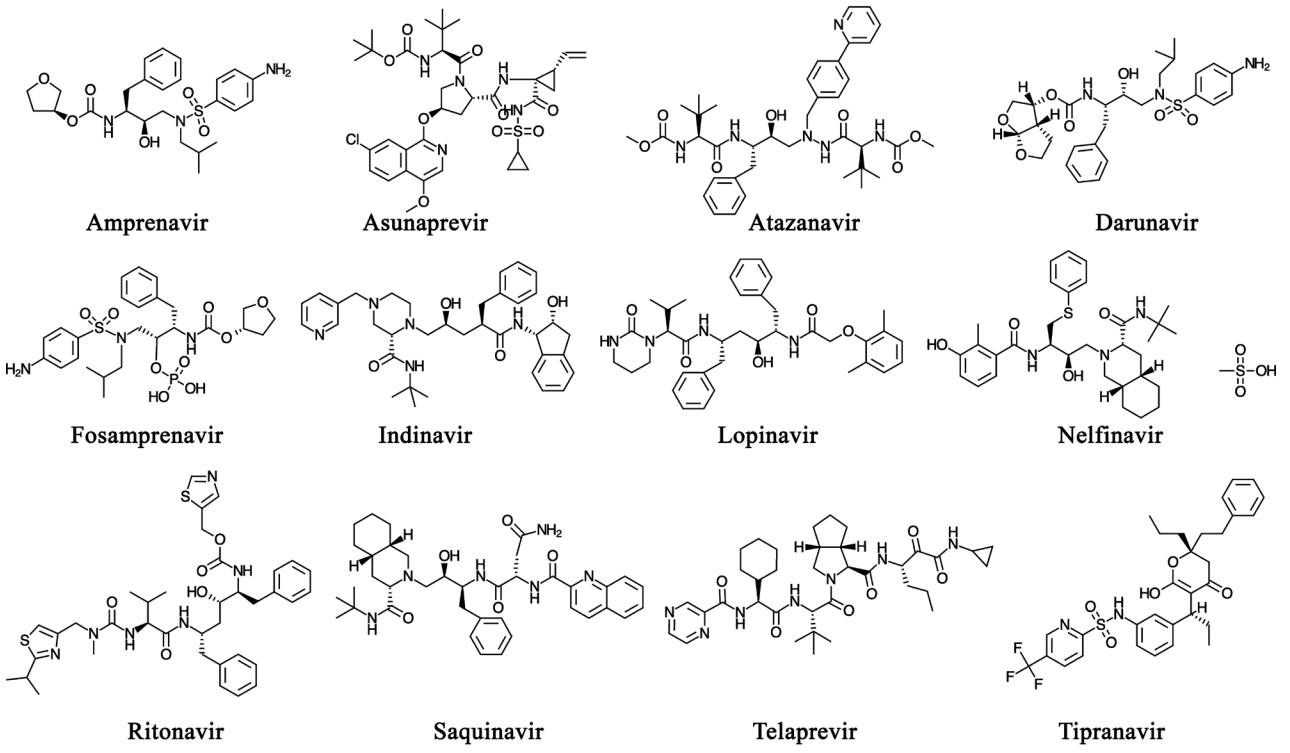

Figure 1. Graphical display of the two-dimensional structures of the potential SARS-CoV-2 protease inhibitors.

protease inhibitors through the consideration of the KID procedure [41] [42] [43] makes the current research as a distinctive improvement over recent similar works on the search of a proper therapy for the COVID-19 disease [44] [45] [46] [47].

2. Computational Methodology

2.1. Molecular Systems Relaxation and Optimization

The molecular structures of the ligands were obtained from the online ZINC15 database [48]. Their structures were geometrically optimized and the most stable conformer in each case was selected. Random sampling was used in the process involving Molecular Mechanics methods with different torsional angles through the overall MMFF94 force field [49] [50] with connection to the MarvinView 17.15 program (ChemAxon, Budapest, Hungary). MarvinView is an advanced chemical viewer that is considered to be suitable for the representation and study of single and multiple chemical structures, reactions, and queries. This was followed by a review of the chemistry involved in the molecular structures and a generation of stereoisomer 3D structures, also by the use of MarvinView 17.15.

After the conformational determination procedure, the selected molecular structures were geometrically reoptimized followed by the analysis of the vibrational frequencies using the Gaussian 09 series of programs [51]. The procedure was performed in the context of the Density Functional Theory (DFT) methodology using the MN12SX density functional [52] and the Def2SVP basis set [53] [54] with the SMD parameterization of the Integral Equation Formalism-Polarized Continuum Model [55] and water as the solvent. The MN12SX density functional was chosen because it is already well known that it is capable of giving very good results for several structural and thermodynamic properties [52]. The resulting model chemistry, MN12SX/Def2TZVP/H2O, has proven to be adequate because MN12SX behaves as a Koopmans-complaint density functional which is a very helpful feature for obtaining accurate HOMO and LUMO orbital energies avoiding the determination of the energies of the cationic and anionic systems for which convergence is usually hard to obtain for the somewhat large molecules as peptides are [41] [42] [43].

2.2. KID Procedure

It is usually assumed that the goodness of a given density functional can be estimated by comparing the results that it gives with the experimental values that are trying to be reproduced or with the results that can be obtained through post Hartree-Fock calculations like MP2, MP4 or CCSD. However, this is not always possible due to the lack of experimental results for the molecular systems that are being studied or the large size of the molecules that keep some accurate methodologies to be computationally practical. For this reason, we have developed a protocol named KID (Koopmans in DFT) [41] [42] [43], which is an attempt to validate a given density functional in terms of its internal coherence. Within

the KID protocol four descriptors have been defined where it has been shown that there is a connection between those descriptors and the simplest conformity to the theorem of Koopmans or the Ionization Energy theorem, which is its equivalent within the Generalized Kohn-Sham (GKS) version of DFT, by connecting ϵ_H to $-I$, ϵ_L to $-A$, and their actions through the HOMO-LUMO gap as $J_I = \left|\epsilon_H + E_{gs}(N-1) - E_{gs}(N)\right|$, $J_A = \left|\epsilon_L + E_{gs}(N) - E_{gs}(N+1)\right|$ and $J_{HL} = \sqrt{J_I^2 + J_A^2}$. An additional descriptor ΔSL has been designed [41] [42] [43] to help in the verification of the accuracy of the KID approximation by comparing the HOMO energy of the radical anion with the energy of the LUMO of the neutral species. Although the Koopmans-complaint behavior of the MN12SX density functional has been proven previously for the case of peptides [41] [42] [43], we think that it is worth to perform a further validation for the case of the molecules considered in the present study.

2.3. Chemical Reactivity Properties

On the basis of the molecular structures obtained from the geometry optimizations, the calculation of the KID parameters as well as the Conceptual DFT-based chemical reactivity descriptors was pursued by resorting to our in-house developed "CDFT" application [41] [42] [43]. The parameters found were the ionization potential (I) and the electron affinity (A), directly from the results of the ground state computed energy, by using the same density functional and basis set as for the optimization step. This was followed by the determination of the global reactivity descriptors, which are: global hardness (η), electronegativity (χ, and electrophilicity (ω) [29] [30] [31]. Also, the electrodonating power (ω^-) and electroaccepting power (ω^+) [39] and finally, the net electrophilicity ($\Delta\omega^\pm$) [56], whose meanings are described as follows:

- Chemical Potential. This property measures the tendency of the electron to escape from systems in equilibrium. It is equal to minus the electronegativity.
- Global Hardness. It quantifies the resistance of a molecule to intramolecular charge transfer.
- Electrophilicity Index. It is defined in terms of the square of chemical potential divided by the chemical hardness and it denotes the stabilization energy after a system gets an additional electronic charge from the external environment.
- Electrodonating Power. It represents the capability of a chemical system to donate a small fractional charge.
- Electroaccepting Power. It represents the capability of a chemical system to accept a small fraction of charge.
- Net Electrophilicity. It is a measure of the relative electrophilicity.

Their mathematical definitions are expressed through the following equations [29] [30] [31] [39] [56]:

Electronegativity $$\chi = -\frac{1}{2}(I + A) \approx \frac{1}{2}(\epsilon_L + \epsilon_H)$$

Global Hardness	$\eta = (I - A) \approx (\epsilon_L - \epsilon_H)$
Electrophilicity	$\omega = \frac{\mu^2}{2\eta} = \frac{(I+A)^2}{4(I-A)} \approx \frac{(\epsilon_L + \epsilon_H)^2}{4(\epsilon_L - \epsilon_H)}$
Electrodonating Power	$\omega^- = \frac{(3I+A)^2}{16(I-A)} \approx \frac{(3\epsilon_H + \epsilon_L)^2}{16\eta}$
Electroaccepting Power	$\omega^+ = \frac{(I+3A)^2}{16(I-A)} \approx \frac{(\epsilon_H + 3\epsilon_L)^2}{16\eta}$
Net Electrophilicity	$\Delta\omega^{\pm} = \omega^+ - (-\omega^-) = \omega^+ + \omega^-$

being ϵ_H and ϵ_L the HOMO and LUMO energies associated with each of the molecules considered in this work.

2.4. Molecular Docking

The crystal structure of COVID-19 main protease related to SARS-CoV-2 with PDB ID: 6M03 has been retrieved from the Protein Data Base (https://www.rcsb.org/structure/6M03) and was considered as the receptor in this study. The molecular docking was performed with the aid of AutoDock 4.2.6 [57]. As a part of the procedure, water molecules were eliminated and only polar hydrogens were added to the protein structure for the simulation process of the intermolecular interactions between the protein and the ligand in the active site. The Lamarckian Genetic Algorithm (LGA) was considered for the estimation of the free energy change upon binding [58].

The grid box for the docking was built with a size of 80 × 80 × 80 points, centered at x = 12.116, y = −11.384 and, z = 4.660 coordinates and a grid spacing of 0.381Å. The size and center of the grid box were defined after a cavities search in the structure that establishes the regions which can be occupied by the ligand. The search was developed by using the CAVER Analyst 2.0 Beta program (CAVER, Pilsen, Czech Republic). The docking parameters used for the LGA based conformational searches are docking trials: 150, population size: 150, the maximum number of energy evaluations: 2,500,000, the maximum number of top individuals to survive to next generation: 1, rate of gene mutation: 0.02, rate of crossover: 0.8: Mean of Cauchy distribution for gene mutation: 0.0, the variance of Cauchy distribution for gene mutation: 1.0, and the number of generations for picking: 10.

3. Results and Discussion

3.1. Geometry Optimization

The starting point consisted in the optimization of the geometries of the twelve inhibitors in the presence of water as the solvent and their vibrational frequencies were analyzed to verify that each molecular structure corresponded to the minimum energy conformations. The resulting optimized structures are shown in **Figure 2**. The structures showed minimal changes from those obtained from the ZINC15 database so it was not considered necessary to display a table with

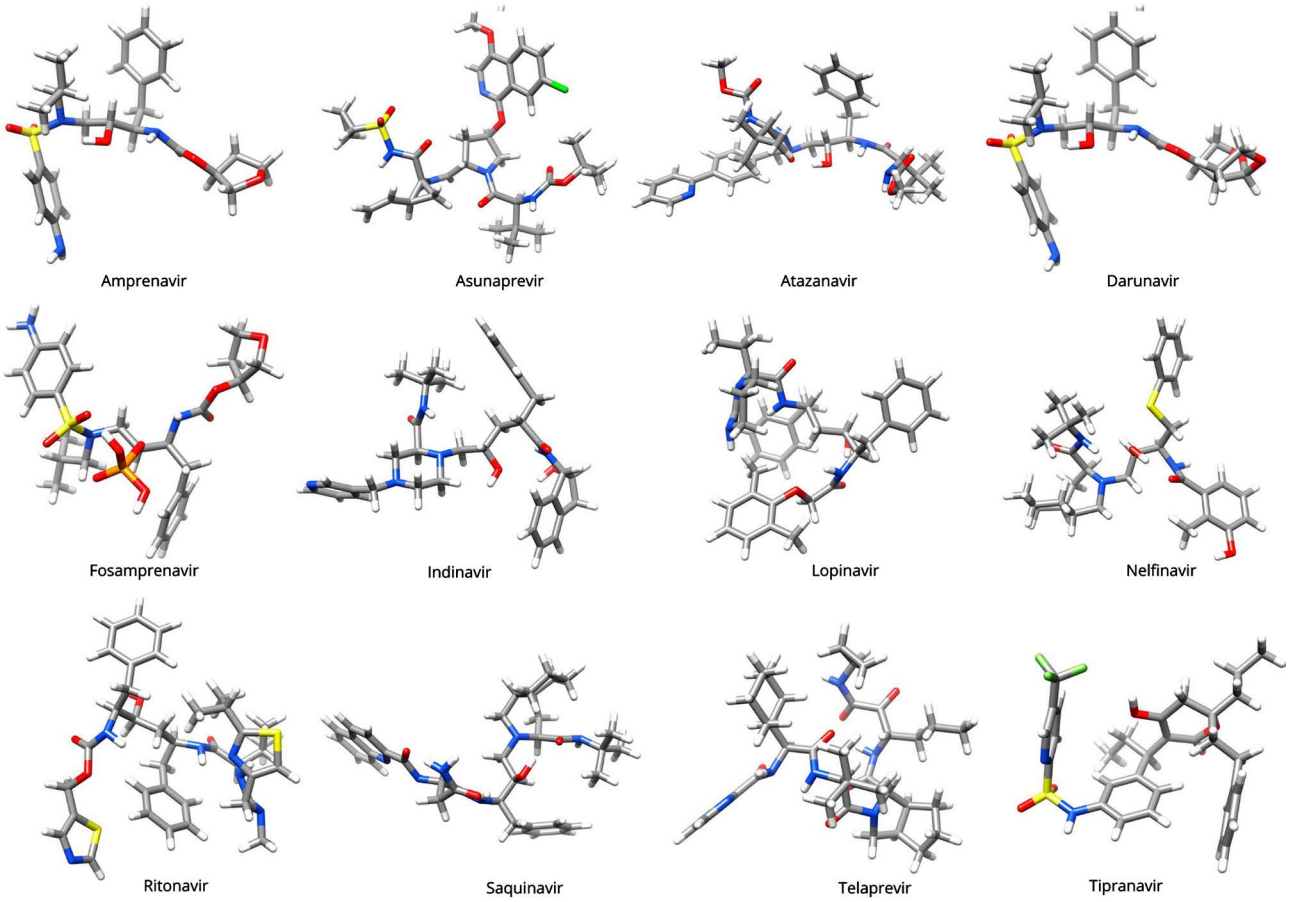

Figure 2. Optimized molecular structures of the inhibitors calculated with MN12SX/Def2SVP with water as the solvent. The color code is: gray for carbon, red for oxygen, blue for nitrogen, yellow for sulfur, orange for phosphorous, green for chlorine, light blue for fluorine and white for hydrogen

the optimized bond and angles.

3.2. KID Procedure Validation

Although the Koopmans-complaint behavior of the MN12SX density functional has been proven previously for the case of peptides [41] [42] [43], we think that it is worth to perform a further validation for the case of the molecules considered in the present study. This determination has been achieved by making use of the in-house developed CDFT software tool and the results of this analysis are shown in Table 1.

It can be seen from the results in Table 1 that the descriptors considered for the estimation of the goodness of the selected density functional through the KID procedure are very close to zero for all the studied molecules, providing an accurate justification for the choice of the MN12SX/Def2DZVP/H2O model chemistry employed for the computational determinations in this study.

3.3. Chemical Reactivity of the SARS-CoV-2 Inhibitors

With the most stable and relaxed molecular structure of the analyzed SARS-CoV-2

inhibitors, the analysis of their reactivity was performed using the descriptors mentioned above and included in Table 2.

The electronic affinities of inhibitors vary from 0.89 to 2.66 eV. The greater facility to form an anion is for Fipranavir. For the case of the ionization potential, Telaprevir is the system with the greatest potential of losing an electron with

Table 1. HOMO, LUMO and SOMO orbital energies, HOMO-LUMO gap and the KID descriptors (all in eV^{-1}) tested in the verification of the Koopmans-like behavior of the MN12SX density functional for the SARS-CoV-2 inhibitors.

Ligand	HOMO	LUMO	SOMO	SOMO	J_I	J_A	J_{HL}	ΔSL
Amprenavir	−6.144	−1.174	−1.116	4.970	0.009	0.029	0.030	0.058
Asunaprevir	−5.844	−1.884	−1.852	3.960	0.032	0.015	0.035	0.032
Atazanavir	−6.318	−1.821	−1.807	4.498	0.022	0.006	0.023	0.013
Darunavir	−6.144	−1.175	−1.118	4.969	0.009	0.028	0.029	0.057
Fosamprenavir	−5.948	−1.015	−0.950	4.933	0.016	0.033	0.037	0.065
Indinavir	−6.257	−1.089	−1.077	5.168	0.058	0.006	0.058	0.012
Lopinavir	−6.551	−0.893	−0.913	6.658	0.008	0.009	0.012	0.020
Nelfinavir	−5.767	−1.733	−1.690	4.034	0.188	0.019	0.190	0.043
Ritonavir	−6.512	−1.463	−1.228	5.049	0.005	0.122	0.122	0.235
Saquinavir	−6.335	−2.650	−2.642	3.684	0.022	0.004	0.022	0.008
Telaprevir	−7.016	−2.616	−2.539	4.400	0.015	0.039	0.042	0.077
Tipranavir	−6.147	−2.659	−2.512	3.489	0.014	0.072	0.074	0.147

Table 2. Global reactivity descriptors for the potential SARS-COVID-2 inhibitors: Electronegativity (χ), Hardness (η), Electrophilicity (ω) (all in eV), Softness S (in eV^{-1}), Nucleophilicity N, Electrodonating Power (ω^-), Elctroaccepting Power (ω^+) and Net Electrophilicity ($\Delta\omega^\pm$) (also in eV).

Ligand	χ	η	ω	S	N	ω^-	ω^+	$\Delta\omega^\pm$
Amprenavir	3.66	4.97	1.35	0.20	2.65	4.83	1.18	6.01
Asunaprevir	3.86	3.96	1.89	0.25	2.95	5.95	2.09	8.04
Atazanavir	4.07	4.50	1.84	0.22	2.47	5.10	1.93	7.93
Darunavir	3.66	4.97	1.35	0.20	2.65	4.84	1.18	6.01
Fosamprenavir	3.48	4.93	1.23	0.20	2.84	4.51	1.02	5.53
Indinavir	3.67	5.17	1.31	0.19	2.54	4.77	1.10	5.87
Lopinavir	3.72	5.66	1.22	0.18	2.24	4.66	0.94	5.60
Nelfinavir	3.75	4.03	1.74	0.25	3.03	5.61	1.86	7.47
Ritonavir	3.99	5.05	1.58	0.20	2.28	5.46	1.47	6.93
Saquinavir	4.49	3.68	2.74	0.27	2.46	7.95	3.46	11.42
Telaprevir	4.82	4.40	2.64	0.23	1.78	7.95	3.14	11.09
Tipranavir	4.40	3.49	2.78	0.29	2.65	7.98	3.57	11.55

a value of 7.02 eV. Chemical Hardness values range from 3.49 to 5.66 eV, This means that Tipranavir with 3.49 eV has the lowest resistance to change its electronic configuration; thus, it will react more easily in the presence of the protease. Electronegativity values are located between 3.48 and 4.49 eV. The inhibitor systems with a bigger tendency to attract electrons are Saquinavir, Tipranavir and Telaprevir respectively.

The Electrophilicity values are in a range of 1.22 to 2.78 eV. This property denotes the capacity to stabilize the energy of a system when it becomes saturated with electrons from the surroundings. The inhibitor which is most capable to stabilize energy is Tipranavir. Also, in all cases, the electrodonating powers or the potential inhibitors are larger than its accepting powers.

As a complement of these global reactivity descriptors that arise from Conceptual DFT [29] [30] [31] [39] [56], Domingo and his collaborators [59] [60] [61] [62] [63] have proposed a Nucleophilicity index N through the consideration of the HOMO energy obtained through the KS scheme with an arbitrary shift of the origin taking the molecule of tetracyanoethylene (TCE) as a reference. On the basis of the previous definition and the scale established by these authors [60], it can be concluded that Nelfinavir can be regarded as a strong nucleophile because the value for the Nucleophilicity N is slightly greater than 3 eV, while the other inhibitors can be considered as moderate nucleophiles with the exception of Telaprevir with a N value of 1.77 eV, thus labeled as a marginal nucleophile.

3.4. Molecular Docking and Active Site Descriptors for the SARS-CoV-2 Inhibitors

The Molecular Docking calculations were performed for the interaction between the protease protein with PDB code 6M03 and twelve potential inhibitors of protease included in the ZINC15 database of the Food and Drug Administration (FDA).

One of the important results that arise from the Molecular Docking process is the binding energy (BE) of the inhibitors. Negative values for this BE are an indication of the stability of the system and for the interaction with the active site of the protein. The docking procedure was evaluated for 10 poses.

The values corresponding to the lowest energy conformation are in a range from −6.85 to −2.11 kcal/mol. The stability decreases in the following order: Indinavir > Lopinavir > Tipranavir > Nelfinavir > Asunaprevir > Telaprevir > Darunavir > Amprenavir > Fosamprenavir > Ritonavir > Atazanavir > Saquinavir.

The other important result from the molecular docking is the description of the active site for each inhibitor. It is important to know the bonding between the analyzed macromolecule and the ligand because if a bond shows a good docking and its functional groups are well positioned so that they interact with the active site of the analyzed macromolecule, then it is likely that this bond is biologically active [64] [65]. This ability of the ligands to bind to macromolecules is directly related to the chemical reactivity properties of the molecular

systems involved. The marginal or strong nucleophilic or electrophilic character defines the interaction of the geometrical interaction structure in the binding pocket of the ligand. The moderate nucleophilic character of most of the ligands can explain the presence of the lysine residue in the active site of almost all of the ligands.

The active site of the macromolecule remains in the core of the protein structure for all the tested inhibitors. Some of the residues are linked together in protein sequences. The residues of the active site for each ligand are presented in Table 3.

There are residues repeated in the contour of the pose with the best score of each ligand. Lysine5 (LYS5) is present in the active site of eight residues: Amprenavir, Darunavir, Fosamprenavir, Indinavir, Nelfinavir, Saquinavir, Telaprevir

Table 3. Binding energies, active sites and interactions between the inhibitors and the main protease of SARS-CoV-2-PDB: 6M03 obtained by the Molecular Docking procedure.

Ligand	Binding Energy (Kcal/mol)	Active Site	Hydrogen Bonds
Amprenavir	−4.95	LYS5, TYR126-GLN127, LYS137, SER139, GLU288-ASP289-GLU290	LYS5-O7 ASP289-N10
Asunaprenavir	−5.64	PHE8, VAL104, ILE106, GLN110-THR111, ASN151-ILE152-ASP153, SER158, THR292, PHE294-ASP295	LYS102-O47
Atanazavir	−3.36	TYR126, LYS137-GLN138-SER139-PHE140, GLY170-VAL171	0
Darunavir	−5.09	LYS5, TRY126-GLN127-ARG131, LYS137-GLY138, ASP289-GLU290	GLU290-O5
Fosamprenavir	−3.94	LYS5, TRY126-GLN127-CYS128, LYS137, LEU286-LEU287-GLU288, ASP289-GLU290	0
Indinavir	−6.85	LYS5, TYR126-GLN127, SER139, GLU290	LYS5-O3 GLU290-O3
Lopinavir	−6.82	PHE8, VAL104-ARG105-ILE106, GLN110-THR111, ASN151, PHE294-ASP295	0
Nelfinavir	−6.15	LYS5, TYR126-GLN127, LYS137-LY138-SER139, PHE140, GLU166, THR169-GLY170	LYS5-O2 GLY138-N8 SER139-O5
Ritonavir	−3.87	LYS102, THR111, ASN151-ILE152, SER158, THR292, PHE294-ASP295, ARG298	0
Saquinavir	−2.11	LYS5, TYR123, LYS137-GLY138, SER139, LUE141, GLU166, HIS172	0
Telaprevir	−5.35	LYS5, TYR126-GLN127, ARG131, LYS137, GLU290	LYS5-O8 LYS5-O51 GLN127-N34 LYS137-N46
Tipranavir	−6.60	LYS5, TYR126-GLY127;LYS137-GLY138-SER139, HIS172, GLU290	GLU290-O6

and Tipranavir. The dipeptide Tyrosine126-Glutamine127 (TYR 126-GLN127) is present in the active site of seven of the antiviral systems: Amprenavir, Darunavir, Fosamprenavir, Indinavir, Nelfinavir, Telaprevir and Tipravir. Lysine137-Glycine138 (LYS137-GLY138) is present in the active site of five residues as Atazanavir, Darunavir, Nelfinavir, Saquinavir, and Tipranavir. And Lysine137 (LYS137) is as simple residue present in three ligands: Amprenavir, Fosamprenavir and Telaprevir. Glutamic acid is present in the active site with six ligands, Amprenavir, Darunavir, Fosaprenavir, Indinavir, Telaprevir and Tipranavir. The active sites of all the ligands are shown in **Figure 3**.

3.5. Hydrogen Bonds

The electrostatic interactions analysis between the ligands and the residues of the active site was performed with the aim of classifying them as strong, moderate or weak following the recommendation of Jeffrey [66]. It could be appreciated that seven of the twelve studied ligands presented hydrogen bonds which can be considered significative because the electrostatic interactions as hydrogen bonds are important as a measure of the highest probability of inhibitory effectiveness. This information is also summarized in **Table 3**.

- Amprenavir—Weak hydrogen bond between O7 of the (C=O) accepting group of the ligand and amino group of LYS5 and with bond distance of 2.24 Å. Moderate hydrogen bonds between carboxylic group of ASP289 and N10 from the amino of the ligand with bond distance of 2.10 Å.

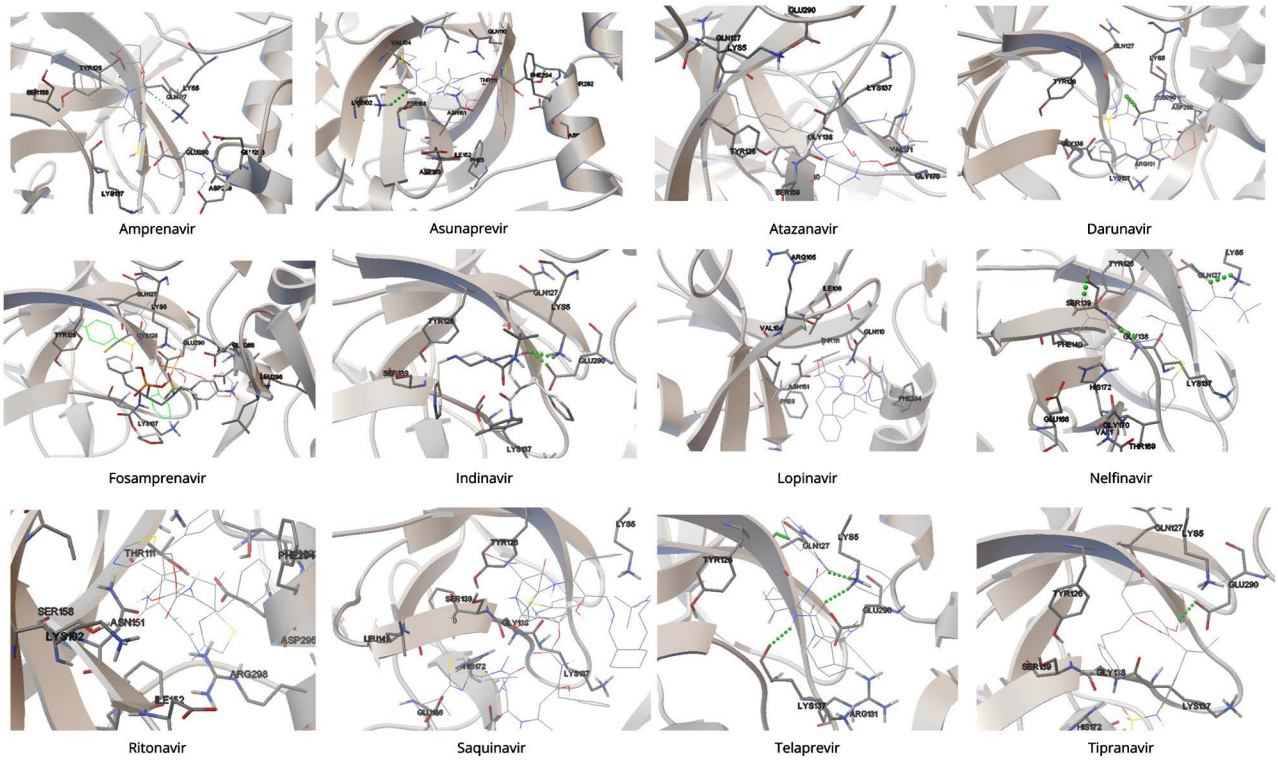

Figure 3. Binding conformations of the amino acids on the active site of the main protease of SARS-CoV-2 (PDB code 6M03) with the inhibitors and hydrogen bond interactions in green dots.

- Asunaprevir—Moderate hydrogen bonds between amino group of LYS102 and O47 of the ligand with bond distance of 1.88 Å.
- Darunavir—Shows a moderate hydrogen bond with the donor group (O-H) belonging the donor group (O-H) belonging the ligand and O5 of carboxylic group of GLU290 with 1.92 Å.
- Indinavir—Moderate hydrogen bond between O3 of the (C=O) accepting group of the ligand and amino group of LYS5 and with bond distance of 2.13 Å. Moderate hydrogen bond between O3 of the (C=O) accepting group of the ligand and amino group of LYS5 and carboxylic group of GLU290 with bond distance of 1.80 Å.
- Nelfinavir—Moderate hydrogen bond between O2 of the (C=O) accepting group of the ligand and amino group of LYS5 and with bond distance of 2.08 Å. Moderate hydrogen bond between O5 of the donor group (O-H) belonging to one of the rings of the ligand and the hydroxymethyl group of SER139 with bond distance of 1.90 Å. Moderate hydrogen bond between N8 of the amine of the ligand and carboxylic group of GLY138. The bond distance is 1.82 Å.
- Telaprevir—Two moderate hydrogen bonds between amino group of LYS5 with O38 and O51 of acceptor groups (C=O) of the ligand. Distances are 1.75 and 1.90 Å respectively. Moderate bond between N34 of the ligand and the secondary amine of GLN127, distance of 2.13 Å. Moderate bond between N46 of the ligand and LYS137, distance of 1.89 Å.
- Tipranavir—Moderate hydrogen bond of acceptor carboxylic group (C=O) of GLU 290 and O6 of the donor group (O-H) of the ligand. Bond distance 2.00 Å.

4. Conclusions

In this research, we have performed the calculation of the chemical reactivity properties and a Molecular Docking study of the main protease proteins of SARS-CoV-2 6M03 with twelve known molecules with recognized inhibitory activity included in the ZINC15 drugs database of the Food and Drug Administration (FDA). Binding energies, hydrogen bonds and residues that form the active site were defined for all the ligands.

The results obtained from the determination of the chemical reactivity parameters indicate that the lowest values for the chemical hardness were for Tipranavir with 3.49 eV, Asunaprevir with 3.96 eV and Nelfinavir with 4.03 eV. This means that these ligands have the lowest resistance to change the shape of their electronic densities, and thus are the most reactive ones. According to the Binding Energy results obtained from the Molecular Docking procedure, Indinavir had the greatest stability with the studied protease followed by Lopinavir, Tipranavir and Nelfinavir with a small binding energy difference. The binding site within the biological target maintained the presence of some residues in simple form and linked in protein arrangements. LYS5, GLU290 and dimer LYS137-

GLY138 residues established interactions with mostly of the ligands and showed electrostatic interactions.

The electrostatic interactions as hydrogen bonds formed are important to define the highest probability of inhibitory effectiveness: Telaprevir, Nelfinavir and Indinavir combined high number of hydrogen bonds with stable conformation Binding Energy. It can be said that these ligands have the highest probability of success for acting as inhibitors of SARS-CoV-2. These results can be the basis for the identification of the best potential compounds for this purpose and could serve as a good starting point for future research in this field.

Acknowledgements

This work was supported by Consejo Nacional de Ciencia y Tecnología (CONACYT) and Centro de Investigación en Materiales Avanzados (CIMAV). NRFH and DGM are researchers from CIMAV and CONACYT.

Conflicts of Interest

The authors declare no conflicts of interest regarding the publication of this paper.

References

[1] Hilgenfeld, R. (2014) From SARS to MERS: Crystallographic Studies on Coronaviral Proteases Enable Antiviral Drug Design. *FEBS Journal*, **281**, 4085-4096. https://doi.org/10.1111/febs.12936

[2] Pillaiyar, T., Manickam, M., Namasivayam, V., Hayashi, Y. and Jung, S.-H. (2016) An Overview of Severe Acute Respiratory Syndrome-Coronavirus (SARS-CoV) 3CL Protease Inhibitors: Peptidomimetics and Small Molecule Chemotherapy. *Journal of Medicinal Chemistry*, **59**, 6595-6628. https://doi.org/10.1021/acs.jmedchem.5b01461

[3] Anand, K. (2003) Coronavirus Main Proteinase (3CLpro) Structure: Basis for Design of Anti-SARS Drugs. *Science*, **300**, 1763-1767. https://doi.org/10.1126/science.1085658

[4] Zhang, L., Lin, D., Sun, X., Curth, U., Drosten, C., Sauerhering, L., Becker, S., Rox, K. and Hilgenfeld, R. (2020) Crystal Structure of SARS-CoV-2 Main Protease Provides a Basis for Design of Improved *α*-Ketoamide Inhibitors. *Science*, **368**, eabb3405. https://doi.org/10.1126/science.abb3405

[5] Borah, P., Deb, P.K., Deka, S., Venugopala, K.N., Singh, V., Mailavaram, R.P., Kalia, K. and Tekade, R.K. (2020) Current Scenario and Future Prospect in the Management of COVID-19. *Current Medicinal Chemistry*. (In Press) https://doi.org/10.2174/0929867327666200908113642

[6] Poater, A. (2020) Michael Acceptors Tuned by the Pivotal Aromaticity of Histidine to Block COVID-19 Activity. *The Journal of Physical Chemistry Letters*, **11**, 6262-6265. https://doi.org/10.1021/acs.jpclett.0c01828

[7] Cavallo, L. and Oliva, R. (2020) D936Y and Other Mutations in the Fusion Core of the SARS-Cov-2 Spike Protein Heptad Repeat 1 Undermine the Post-Fusion Assembly. https://doi.org/10.1101/2020.06.08.140152

[8] da Silva Hage-Melim, L.I., Federico, L.B., de Oliveira, N.K.S., Francisco, V.C.C.,

Correia, L.C., de Lima, H.B., Gomes, S.Q., Barcelos, M.P., Francischini, I.A.G. and de Paula da Silva, C.H.T. (2020) Virtual Screening, ADME/Tox Predictions and the Drug Repurposing Concept for Future Use of Old Drugs against the COVID-19. *Life Sciences*, **256**, Article ID: 117963. https://doi.org/10.1016/j.lfs.2020.117963

[9] Sternberg, A., McKee, D.L. and Naujokat, C. (2020) Novel Drugs Targeting the SARS-CoV-2/COVID-19 Machinery. *Current Topics in Medicinal Chemistry*, **20**, 1423-1433. https://doi.org/10.2174/1568026620999200517043137

[10] Fernández-García, M. (2015) Fármacos Inhibidores de Proteasas Virales. Universidad Complutense de Madrid, Madrid.

[11] Dong, E., Du, H. and Gardner, L. (2020) An Interactive WEB-Based Dashboard to Track COVID-19 in Real Time. *The Lancet Infectious Diseases*, **20**, 533-534. https://doi.org/10.1016/S1473-3099(20)30120-1

[12] Karthick, T. and Tandon, P. (2016) Computational Approaches to Find the Active Binding Sites of Biological Targets against Busulfan. *Journal of Molecular Modeling*, **22**, 142. https://doi.org/10.1007/s00894-016-3015-z

[13] Cumming, J.G., Davis, A.M., Muresan, S., Haeberlein, M. and Chen, H. (2013) Chemical Predictive Modelling to Improve Compound Quality. *Nature Reviews Drug Discovery*, **12**, 948-962. https://doi.org/10.1038/nrd4128

[14] van Tamelen, E.E. (1956) Progress in the Chemistry of Organic Natural Products. *Journal of the American Chemical Society*, **78**, 1266-1266. https://doi.org/10.1021/ja01587a062

[15] Yu, R., Chen, L., Lan, R., Shen, R. and Li, P. (2020) Computational Screening of Antagonists against the SARS-CoV-2 (COVID-19) Coronavirus by Molecular Docking. *International Journal of Antimicrobial Agents*, **56**, Article ID: 106012. https://doi.org/10.1016/j.ijantimicag.2020.106012

[16] Sencanski, M., Perovic, V., Pajovic, S.B., Adzic, M., Paessler, S. and Glisic, S. (2020) Drug Repurposing for Candidate SARS-CoV-2 Main Protease Inhibitors by a Novel *in Silico* Method. *Molecules*, **25**, 3830. https://doi.org/10.3390/molecules25173830

[17] Yamamoto, N., Matsuyama, S., Hoshino, T. and Yamamoto, N. (2020) Nelfinavir Inhibits Replication of Severe Acute Respiratory Syndrome Coronavirus 2 *in Vitro*. https://doi.org/10.1101/2020.04.06.026476

[18] Sterling, T. and Irwin, J.J. (2015) ZINC 15—Ligand Discovery for Everyone. *Journal of Chemical Information and Modeling*, **55**, 2324-2337. https://doi.org/10.1021/acs.jcim.5b00559

[19] Shen, C.-H., Wang, Y.-F., Kovalevsky, A.Y., Harrison, R.W. and Weber, I.T. (2010) Amprenavir Complexes with HIV-1 Protease and Its Drug-Resistant Mutants Altering Hydrophobic Clusters. *FEBS Journal*, **277**, 3699-3714. https://doi.org/10.1111/j.1742-4658.2010.07771.x

[20] Reviriego, C. (2012) Asunaprevir. *Drugs of the Future*, **37**, 247-254. https://doi.org/10.1358/dof.2012.037.04.1789350

[21] Piliero, P.J. (2002) Atazanavir: A Novel HIV-1 Protease Inhibitor. *Expert Opinion on Investigational Drugs*, **11**, 1295-1301. https://doi.org/10.1517/13543784.11.9.1295

[22] Prashantha, C., Gouthami, K., Lavanya, L., Bhavanam, S., Jakhar, A., Shakthiraju, R., Suraj, V., Sahana, K., Sujana, H., Guruprasad, N. and Ramachandra, R. (2021) Molecular Screening of Antimalarial, Antiviral, Anti-Inflammatory and HIV Protease Inhibitors against Spike Glycoprotein of Coronavirus. *Journal of Molecular Graphics and Modelling*, **102**, Article ID: 107769. https://doi.org/10.1016/j.jmgm.2020.107769

[23] Eron, J., Yeni, P., Gathe, J., Estrada, V., DeJesus, E., Staszewski, S., Lackey, P., Katlama, C., Young, B., Yau, L., Sutherland-Phillips, D., Wannamaker, P., Vavro, C., Patel, L., Yeo, J. and Shaefer, M. (2006) The KLEAN Study of Fosamprenavir-Ritonavir versus Lopinavir-Ritonavir, Each in Combination with Abacavir-Lamivudine, for Initial Treatment of HIV Infection over 48 Weeks: A Randomised Non-Inferiority Trial. *The Lancet*, **368**, 476-482. https://doi.org/10.1016/S0140-6736(06)69155-1

[24] Fischer, J. (2006) Analogue-Based Drug Discovery. Wiley-VCH, Weinheim. https://doi.org/10.1002/3527608001

[25] Zhang, K.E., Wu, E., Patick, A.K., Kerr, B., Zorbas, M., Lankford, A., Kobayashi, T., Maeda, Y., Shetty, B. and Webber, S. (2001) Circulating Metabolites of the Human Immunodeficiency Virus Protease Inhibitor Nelfinavir in Humans: Structural Identification, Levels in Plasma, and Antiviral Activities. *Antimicrobial Agents and Chemotherapy*, **45**, 1086-1093. https://doi.org/10.1128/AAC.45.4.1086-1093.2001

[26] Revill, P., Serradell, N., Bolós, J. and Rosa, E. (2007) Telaprevir. *Drugs of the Future*, **32**, 788. https://doi.org/10.1358/dof.2007.032.09.1138229

[27] Doyon, L., Tremblay, S., Bourgon, L., Wardrop, E. and Cordingley, M.G. (2005) Selection and Characterization of HIV-1 Showing Reduced Susceptibility to the Non-Peptidic Protease Inhibitor Tipranavir. *Antiviral Research*, **68**, 27-35. https://doi.org/10.1016/j.antiviral.2005.07.003

[28] Zhang, B., Zhao, Y., Jin, Z., Liu, X., Yang, H. and Rao, Z. (2020) The Crystal Structure of COVID-19 Main Protease in Apo Form. https://doi.org/10.2210/pdb6m03/pdb

[29] Parr, R. and Yang, W. (1989) Density-Functional Theory of Atoms and Molecules. Oxford University Press, New York.

[30] Chermette, H. (1999) Chemical Reactivity Indexes in Density Functional Theory. *Journal of Computational Chemistry*, **20**, 129-154. https://doi.org/10.1002/(SICI)1096-987X(19990115)20:1<129::AID-JCC13>3.0.CO;2-A

[31] Geerlings, P., De Proft, F. and Langenaeker, W. (2003) Conceptual Density Functional Theory. *Chemical Reviews*, **103**, 1793-1873. https://doi.org/10.1021/cr990029p

[32] Geerlings, P., Chamorro, E., Chattaraj, P.K., Proft, F.D., Gázquez, J.L., Liu, S., Morell, C., Toro-Labbé, A., Vela, A. and Ayers, P. (2020) Conceptual Density Functional Theory: Status, Prospects, Issues. *Theoretical Chemistry Accounts*, **139**, Article No. 36. https://doi.org/10.1007/s00214-020-2546-7

[33] Gázquez, J.L. (2009) Chemical Reactivity Concepts in Density Functional Theory. In: Chattaraj, P.K. Ed., *Chemical Reactivity Theory*: *A Density Functional View*, CRC Press, Taylor & Francis Group, Boca Raton, Ch. 2, 7-22. https://doi.org/10.1201/9781420065442.ch2

[34] Basak, S.C., Mills, D., Natarajan, R. and Gute, B.D. (2009) Predicting Chemical Reactivity and Bioactivity of Molecules from Structure. In: Chattaraj, P.K. Ed., *Chemical Reactivity Theory*: *A Density Functional View*, CRC Press, Taylor & Francis Group, Boca Raton, Ch. 31, 479-502. https://doi.org/10.1201/9781420065442.ch31

[35] Toro-Labbé, A., Gutiérrez-Oliva, S., Politzer, P. and Murray, J.S. (2009) Reaction Force: A Rigorously Defined Approach to Analyzing Chemical and Physical Processes. In: Chattaraj, P.K. Ed., *Chemical Reactivity Theory*: *A Density Functional View*, CRC Press, Taylor & Francis Group, Boca Raton, Ch. 21, 293-302. https://doi.org/10.1201/9781420065442.ch21

[36] Matito, E., Poater, J., Solá, M. and von Ragué Schleyer, P. (2009) Aromaticity and Chemical Reactivity. In: Chattaraj, P.K. Ed., *Chemical Reactivity Theory*: *A Density Functional View*, CRC Press, Taylor & Francis Group, Boca Raton, Ch. 28, 419-438. https://doi.org/10.1201/9781420065442.ch28

[37] Chakraborty, A., Pan, S. and Chattaraj, P.K. (2012) Biological Activity and Toxicity: A Conceptual DFT Approach. In: *Structure and Bonding*, Springer, Berlin, 143-179. https://doi.org/10.1007/978-3-642-32750-6_5

[38] Chattaraj, P., Sarkar, U. and Roy, D. (2006) Electrophilicity Index. *Chemical Reviews*, **106**, 2065-2091. https://doi.org/10.1021/cr040109f

[39] Gázquez, J., Cedillo, A. and Vela, A. (2007) Electrodonating and Electroaccepting Powers. *Journal of Physical Chemistry A*, **111**, 1966-1970. https://doi.org/10.1021/jp065459f

[40] Rosales-Hernández, M.C. and Correa-Basurto, J. (2015) The Importance of Employing Computational Resources for the Automation of Drug Discovery. *Expert Opinion on Drug Discovery*, **10**, 213-219. https://doi.org/10.1517/17460441.2015.1005071

[41] Flores-Holgun, N., Frau, J. and Glossman-Mitnik, D. (2020) A Fast and Simple Evaluation of the Chemical Reactivity Properties of the Pristinamycin Family of Antimicrobial Peptides. *Chemical Physics Letters*, **739**, Article ID: 137021. https://doi.org/10.1016/j.cplett.2019.137021

[42] Flores-Holgun, N., Frau, J. and Glossman-Mitnik, D. (2020) Conceptual DFT-Based Computational Peptidology of Marine Natural Compounds: Discodermins A-H. *Molecules*, **25**, 4158. https://doi.org/10.3390/molecules25184158

[43] Flores-Holgun, N., Frau, J. and Glossman-Mitnik, D. (2020) Virtual Screening of Marine Natural Compounds by Means of Chemoinformatics and CDFT-Based Computational Peptidology. *Marine Drugs*, **18**, 478. https://doi.org/10.3390/md18090478

[44] Komatsu, T.S., Okimoto, N., Koyama, Y.M., Hirano, Y., Morimoto, G., Ohno, Y. and Taiji, M. (2020) Drug Binding Dynamics of the Dimeric SARS-CoV-2 Main Protease, Determined by Molecular Dynamics Simulation. *Scientific Reports*, **10**, Article No. 16986. https://doi.org/10.1038/s41598-020-74099-5

[45] Sang, P., Tian, S.-H., Meng, Z.-H. and Yang, L.-Q. (2020) Anti-HIV Drug Repurposing against SARS-CoV-2. *RSC Advances*, **10**, 15775-15783. https://doi.org/10.1039/D0RA01899F

[46] Ngo, S.T., Pham, N.Q.A., Le, L.T., Pham, D.-H. and Vu, V.V. (2020) Computational Determination of Potential Inhibitors of SARS-CoV-2 Main Protease. *Journal of Chemical Information and Modeling*. https://doi.org/10.1021/acs.jcim.0c00491

[47] Kumar, S., Sharma, P.P., Shankar, U., Kumar, D., Joshi, S.K., Pena, L., Durvasula, R., Kumar, A., Kempaiah, P., Poonam and Rathi, B. (2020) Discovery of New Hydroxyethylamine Analogs against 3CLpro Protein Target of SARS-CoV-2: Molecular Docking, Molecular Dynamics Simulation, and Structure-Activity Relationship Studies. *Journal of Chemical Information and Modeling*. https://doi.org/10.1021/acs.jcim.0c00326

[48] Irwin, J.J., Sterling, T., Mysinger, M.M., Bolstad, E.S., Coleman, R.G. (2012) ZINC: A Free Tool to Discover Chemistry for Biology. *Journal of Chemical Information and Modeling*, **52**, 1757-1768. https://doi.org/10.1021/ci3001277

[49] Halgren, T.A. (1996) Merck Molecular Force Field. I. Basis, Form, Scope, Parameterization, and Performance of MMFF94. *Journal of Computational Chemistry*, **17**, 490-519.

https://doi.org/10.1002/(SICI)1096-987X(199604)17:5/6<490::AID-JCC1>3.0.CO;2-P

[50] Halgren, T.A. (1996) Merck Molecular Force Field. II. MMFF94 van der Waals and Electrostatic Parameters for Intermolecular Interactions. *Journal of Computational Chemistry*, **17**, 520-552. https://doi.org/10.1002/(SICI)1096-987X(199604)17:5/6<520::AID-JCC2>3.0.CO;2-W

[51] Frisch, M.J., Trucks, G.W., Schlegel, H.B., Scuseria, G.E., Robb, M.A., Cheeseman, J.R., Scalmani, G., Barone, V., Mennucci, B., Petersson, G.A., Nakatsuji, H., Caricato, M., Li, X., Hratchian, H.P., Izmaylov, A.F., Bloino, J., Zheng, G., Sonnenberg, J.L., Hada, M., Ehara, M., Toyota, K., Fukuda, R., Hasegawa, J., Ishida, M., Nakajima, T., Honda, Y., Kitao, O., Nakai, H., Vreven, T., Montgomery Jr., J.A., Peralta, J.E., Ogliaro, F., Bearpark, M., Heyd, J.J., Brothers, E., Kudin, K.N., Staroverov, V.N., Kobayashi, R., Normand, J., Raghavachari, K., Rendell, A., Burant, J.C., Iyengar, S.S., Tomasi, J., Cossi, M., Rega, N., Millam, J.M., Klene, M., Knox, J.E., Cross, J.B., Bakken, V., Adamo, C., Jaramillo, J., Gomperts, R., Stratmann, R.E., Yazyev, O., Austin, A.J., Cammi, R., Pomelli, C., Ochterski, J.W., Martin, R.L., Morokuma, K., Zakrzewski, V.G., Voth, G.A., Salvador, P., Dannenberg, J.J., Dapprich, S., Daniels, A.D., Farkas, O., Foresman, J.B., Ortiz, J.V., Cioslowski, J. and Fox, D.J. (2016) Gaussian 09 Revision E.01. Gaussian Inc., Wallingford.

[52] Peverati, R. and Truhlar, D.G. (2012) Screened-Exchange Density Functionals with Broad Accuracy for Chemistry and Solid-State Physics. *Physical Chemistry Chemical Physics*, **14**, 16187-16191. https://doi.org/10.1039/c2cp42576a

[53] Weigend, F. and Ahlrichs, R. (2005) Balanced Basis Sets of Split Valence, Triple Zeta Valence and Quadruple Zeta Valence Quality for H to Rn: Design and Assessment of Accuracy. *Physical Chemistry Chemical Physics*, **7**, 3297-3305. https://doi.org/10.1039/b508541a

[54] Weigend, F. (2006) Accurate Coulomb-Fitting Basis Sets for H to R. *Physical Chemistry Chemical Physics*, **8**, 1057-1065. https://doi.org/10.1039/b515623h

[55] Marenich, A., Cramer, C. and Truhlar, D. (2009) Universal Solvation Model Based on Solute Electron Density and a Continuum Model of the Solvent Defined by the Bulk Dielectric Constant and Atomic Surface Tensions. *Journal of Physical Chemistry B*, **113**, 6378-6396. https://doi.org/10.1021/jp810292n

[56] Chattaraj, P., Chakraborty, A. and Giri, S. (2009) Net Electrophilicity. *Journal of Physical Chemistry A*, **113**, 10068-10074. https://doi.org/10.1021/jp904674x

[57] Morris, G.M., Huey, R., Lindstrom, W., Sanner, M.F., Belew, R.K., Goodsell, D.S. and Olson, A.J. (2009) AutoDock4 and AutoDockTools4: Automated Docking with Selective Receptor Flexibility. *Journal of Computational Chemistry*, **30**, 2785-2791. https://doi.org/10.1002/jcc.21256

[58] Morris, G.M., Goodsell, D.S., Halliday, R.S., Huey, R., Hart, W.E., Belew, R.K. and Olson, A.J. (1998) Automated Docking Using a Lamarckian Genetic Algorithm and an Empirical Binding Free Energy Function. *Journal of Computational Chemistry*, **19**, 1639-1662. https://doi.org/10.1002/(SICI)1096-987X(19981115)19:14<1639::AID-JCC10>3.0.CO;2-B

[59] Domingo, L.R., Chamorro, E. and Perez, P. (2008) Understanding the Reactivity of Captodative Ethylenes in Polar Cycloaddition Reactions. A Theoretical Study. *The Journal of Organic Chemistry*, **73**, 4615-4624. https://doi.org/10.1021/jo800572a

[60] Jaramillo, P., Domingo, L.R., Chamorro, E. and Pérez, P. (2008) A Further Exploration of a Nucleophilicity Index Based on the Gas-Phase Ionization Potentials. *Journal of Molecular Structure: THEOCHEM*, **865**, 68-72. https://doi.org/10.1016/j.theochem.2008.06.022

[61] Domingo, L.R. and Sáez, J.A. (2009) Understanding the Mechanism of Polar Diels-Alder Reactions. *Organic and Biomolecular Chemistry*, **7**, 3576-3583. https://doi.org/10.1039/b909611f

[62] Domingo, L.R. and Perez, P. (2011) The Nucleophilicity N Index in Organic Chemistry. *Organic and Biomolecular Chemistry*, **9**, 7168-7175. https://doi.org/10.1039/c1ob05856h

[63] Domingo, L.R., Ríos-Gutiérrez, M. and Pérez, P. (2016) Applications of the Conceptual Density Functional Theory Indices to Organic Chemistry Reactivity. *Molecules*, **21**, 748. https://doi.org/10.3390/molecules21060748

[64] Thomas, G. (2003) Fundamentals of Medicinal Chemistry. J. Wiley & Sons, New York.

[65] Patrick, G.L. (2013) An Introduction to Medicinal Chemistry. Oxford University Press, Oxford.

[66] Jeffrey, G. (1997) An Introduction to Hydrogen Bonding. Oxford University Press, New York.